Journal of Power Sources 328 (2016) 463–471

Contents lists available at ScienceDirect

Journal of Power Sources

journal homepage: www.elsevier.com/locate/jpowsour

Gold supported on zirconia polymorphs for hydrogen generation from formic acid in base-free aqueous medium

Qing-Yuan Bi [a, b], Jian-Dong Lin [a], Yong-Mei Liu [a], He-Yong He [a], Fu-Qiang Huang [b, c], Yong Cao [a, *]

[a] Department of Chemistry, Shanghai Key Laboratory of Molecular Catalysis and Innovative Materials, Collaborative Innovation Center of Chemistry for Energy Materials, Fudan University, Shanghai, 200433, PR China
[b] State Key Laboratory of High Performance Ceramics and Superfine Microstructure, Shanghai Institute of Ceramics, Chinese Academy of Sciences, Shanghai, 200050, PR China
[c] Beijing National Laboratory for Molecular Sciences and State Key Laboratory of Rare Earth Materials Chemistry and Applications, College of Chemistry and Molecular Engineering, Peking University, Beijing, 100871, PR China

HIGHLIGHTS

- ZrO_2 polymorphs possess markedly different amount of surface acidity and basicity.
- The basic sites of gold catalyst are crucial for the cleavage of O–H bond of HCOOH.
- Au/m-ZrO_2 shows excellent reaction rate of 81.8 L H_2 g_{Au}^{-1} h^{-1}.
- The H/D exchange between HCOOH and H_2O in reaction system is observed.

ARTICLE INFO

Article history:
Received 18 May 2016
Received in revised form
28 July 2016
Accepted 10 August 2016
Available online 17 August 2016

Keywords:
Gold catalysis
Zirconia polymorphs
Formic acid
Base-free
Hydrogen

ABSTRACT

Formic acid (FA) has attracted considerable attention as a safe and convenient hydrogen storage material for renewable energy transformation. However, development of an efficient heterogeneous catalyst for selective FA decomposition for ultraclean H_2 gas in the absence of any alkalis or additives under mild conditions remains a major challenge. Based on our previous work on Au/ZrO_2 as a robust and efficient catalyst for FA dehydrogenation in amine system, we report here ZrO_2 with different nanocrystal polymorphs supported Au nanoparticles can achieve near completion of FA dehydrogenation in base-free aqueous medium. Of significant importance is that an excellent rate of up to 81.8 L H_2 g_{Au}^{-1} h^{-1} in open system and highly pressurized gas of 5.9 MPa in closed one can be readily attained at 80 °C for Au/*m*-ZrO_2. *In situ* diffuse reflectance infrared Fourier transform (DRIFT) and CO_2-temperature programmed desorption (TPD) techniques revealed that Au/*m*-ZrO_2 exhibits a higher density of surface basic sites than Au/*t*-ZrO_2 and Au/*a*-ZrO_2. Basic sites in surface can substantially facilitate crucial FA deprotonation process which appears to be a key factor for achieving high dehydrogenation activity. The H/D exchange between solvent of H_2O and substrate of FA was observed by the kinetic isotope effect experiments.

1. Introduction

Hydrogen is considered as a promising alternative to satisfy the increasing demands for an efficient and clean energy supply [1–4]. However, the practical realizations of controlled storage and release of hydrogen are still of great challenges in the fuel cell based hydrogen economy [5,6]. To date, chemical methods for hydrogen storage and use have focused on the use of metal hydrides [7], liquid organic heterocycles (LOH) [8], ammonia borane (AB) [9], alcohols [10], hydrazine [11] et al. as storage materials. Of special interest is the use of bio-renewable formic acid (FA) as hydrogen carrier, not only due to its role in sustainable energy production and renewable chemical synthesis but also for its simplicity which makes it ideal for fundamental bond making and breaking studies [12–15]. It was identified that the decomposition of FA may occur via two distinct reaction pathways, namely the decarboxylation,

* Corresponding author.
E-mail address: yongcao@fudan.edu.cn (Y. Cao).

http://dx.doi.org/10.1016/j.jpowsour.2016.08.056
0378-7753/

yielding H_2 and CO_2 (HCOOH(l) → H_2(g) + CO_2(g), $\Delta G_{298\ K} = -35.0$ kJ mol^{-1}) or the dehydration into H_2O and CO (HCOOH(l) → H_2O(l) + CO(g), $\Delta G_{298\ K} = -14.9$ kJ mol^{-1}) [16]. Particularly given that the gravimetric energy density of FA is by a factor of 7 superior compared to commercially available lithium ion batteries, FA thus represents a convenient liquid hydrogen carrier in fuel cells designed for portable use [17]. This has prompted great efforts directed toward the catalytic FA decomposition in the liquid phase, where the production of CO-free H_2 at convenient temperatures is of great importance.

Indeed, much progress has been made in the catalytic dehydrogenation of FA by using homogeneous systems, such as Ru [18,19], Ir [20,21], Rh [22], and Fe complexes [23,24]. However, apart from the practical inconvenience arising from the use of sophisticated and expensive ligands, the widespread application of these systems has been severely limited by the intrinsic air-instability and short recyclability. Therefore, tremendous efforts have been devoted to synthesizing high performance solid catalysts. Among different heterogeneous catalyst systems, mono-, bi- and tri-metal active components have been demonstrated as a series of very effective catalysts for hydrogen evolution via FA decomposition due to simple operation, significant durability, and cost-saving [25–35]. Despite their high performance for dehydrogenation, most reaction processes suffering from indispensable additives of various inorganic alkali (sodium or potassium salts), which can lower the gravimetric energy density of FA [27–30,36–39]. From the standpoint of practical application, the use of additive-free aqueous FA as the liquid chemical hydrogen storage material would be beneficial for maximizing the overall deliverable capacity [25,26,31–35]. Moreover, the ultraclean H_2 gas generated from the FA system would also be advantageous to its direct downstream application of fuel-cell-based technologies for clean power generation [40]. Thus, the development of simple, efficient, and recyclable heterogeneous catalyst system for affording facile and selective evolution of ultrapure H_2 gas (CO < 10 ppm) from FA in base-free aqueous medium under ambient conditions is highly desired.

Gold-containing catalysts have been extensively employed in past decades for low temperature CO oxidation [41], water-gas shift reactions (WGSR) [42], selective oxidation/reduction [43], and fine chemical synthesis [44]. It is also established that gold catalysts are very selective for vapor-phase FA dehydrogenation and gold-based alloy or core-shell structured materials are highly effective for liquid-phase FA decomposition for pure H_2 gas [12,14,26,27,33,35]. During the search for a readily available, applicable, highly active and reusable catalyst for FA dehydrogenation, we have recently found that a simple Au-based catalyst comprising ultrasmall Au nanoclusters dispersed on a biphasic ZrO_2 can efficiently release CO-free H_2 from a FA-amine mixture with controlled manner under ambient conditions, even at room temperature of 25 °C [45]. Although the important role played by ZrO_2 in dehydrogenation was noticed when comparing the activity of Au/ZrO_2 with gold supported on other metal oxides, the fundamental understanding of the essential role of the underlying support, in particular the amphoteric nature of ZrO_2 with different pure crystallite phases, on the origin of the high catalytic activity of Au/ZrO_2 system is still lacking.

Herein, we report Au nanoparticles (NPs) supported on ZrO_2 with different crystal phases and their catalytic properties for additive-free FA dehydrogenation in the aqueous medium under near ambient conditions. Given the well established fact that polymorphic nature of ZrO_2 strongly influences the performance of a ZrO_2-based catalyst, the present work aims to identify the crystalline-phase-dependent behavior of the Au/ZrO_2 systems. To gain an insight into the respective nature of Au and ZrO_2 phases as well as the structural properties of the Au/ZrO_2 catalyst in relation to their performance in base-free FA decomposition, extensive characterization by N_2 adsorption, X-ray diffraction (XRD), temperature programmed desorption (TPD), transmission electron microscopy (TEM), high-angle annular dark-field scanning transmission electron microscopy (HAADF-STEM), X-ray photoelectron spectroscopy (XPS), and diffuse reflectance infrared Fourier transform spectroscopy (DRIFTS) has been carried out.

2. Experimental

2.1. Catalyst preparation

Monoclinic (*m*-) and tetragonal (*t*-) ZrO_2 samples were synthesized at 160 °C for 20 h in a Teflonlined stainless-steel autoclave (250 mL) containing solutions (80 mL) of $CO(NH_2)_2$ (Aldrich, 99.5%) and $ZrO(NO_3)_2$ (Alfa Aesar, 99%) [46]. Deionized water and CH_3OH (Aldrich, 99.9%) were used as solvents for synthesizing *m*-ZrO_2 and *t*-ZrO_2, respectively. The concentration of Zr^{4+} in the solution was 0.4 M, and the $CO(NH_2)_2/Zr^{4+}$ molar ratio was controlled to be 10. The resulting precipitates were respectively washed thoroughly with water and CH_3OH, and dried at 100 °C overnight and calcined at 400 °C for 4 h in air. The amorphous (*a*-) ZrO_2 was prepared by a conventional precipitation method following the reported procedure [45]. Briefly, appropriate amount of $ZrO(NO_3)_2$ was dissolved in 200 mL deionized water, the pH was adjusted to about 9.5 by dropwise addition of 2.5 M $NH_3 \cdot H_2O$ (Aldrich, 28%) under stirring at 25 °C. The resultant hydrogel was washed with deionized water after stirring for 8 h. The precipitate was then dried at 100 °C overnight followed by calcination at 300 °C in air for 2 h to obtain the final material. The biphasic ZrO_2 (*b*-ZrO_2, 56% monoclinic phase and 44% tetragonal phase) was prepared following the above-mentioned procedure of *a*-ZrO_2 but using oxychloride octahydrate ($ZrOCl_2 \cdot 8H_2O$) as the zirconium precursor and 400 °C as the final calcination temperature.

A modified deposition-precipitation (DP) procedure has been used to prepare the Au/ZrO_2 samples [45]. Briefly, 2.0 g ZrO_2 powders were dispersed into 100 mL 1 mM of aqueous solution of $HAuCl_4$ (Alfa Aesar, 48 wt% Au), the pH was adjusted to 9.0 by dropwise addition of 0.25 M $NH_3 \cdot H_2O$ (CAUTION: the addition of $NH_3 \cdot H_2O$ to $HAuCl_4$ solution probably give rise to highly explosive fulminating gold). After stirring for 6 h at 25 °C, the catalyst was washed several times with deionized water until free of chloride ions (using $AgNO_3$ solution for test) and separated by filtration. The samples were dried at 100 °C in air for 1 h, and followed by a careful reduction treatment with a stream of 5 vol% H_2/Ar at 300 °C for 2 h.

2.2. Catalyst characterization

Actual Au loading of the catalysts was measured by inductively coupled plasma atomic emission spectroscopy (ICP-AES) using a Thermo Electron IRIS Intrepid II XSP spectrometer. The BET specific surface areas of the prepared catalysts were determined by adsorption–desorption of nitrogen at liquid nitrogen temperature, using a Micromeritics TriStar 3000 equipment. Sample degassing was carried out at 300 °C prior to acquiring the adsorption isotherm. The XRD information of the catalysts was carried out on a German Bruker D8 Advance X-ray diffractometer using nickel filtered Cu Kα radiation at 40 kV and 20 mA, and the crystallite size was calculated according to the Scherrer Equation $D = 0.89\lambda/B\cos\theta$ ($\lambda = 0.154056$ nm). XPS data were recorded with a Perkin Elmer PHI 5000C system equipped with a hemispherical electron energy analyzer. The spectrometer was operated at 15 kV and 20 mA, and a magnesium anode (Mg Kα, $h\nu = 1253.6$ eV) was used. The C 1s line (284.6 eV) was used as the reference to calculate the binding

energies (BE). A JEOL 2011 microscope operating at 200 kV equipped with an EDX unit (Si(Li) detector) was used for the TEM investigations. HAADF-STEM images were obtained on a JEM 2100F electron microscope equipped with an EDX unit and a field-emission-gun (FEG) operated at 200 kV and using a HAADF detector. The samples for electron microscopy were prepared by grinding and subsequent dispersing the powder in ethanol and applying a drop of very dilute suspension on carbon-coated grids.

CO concentration with very low levels can be reliably measured by using a gas chromatograph (Agilent 6890 GC) analysis system equipped with a methanizer and a flame ionization detector (FID, detection limit ~ 1.0 ppmv). More details can be found elsewhere [45].

The basicity of sample was determined by CO_2-TPD experiment. Prior to adsorption of CO_2, the sample (0.1 g) was pretreated at 200 °C for 60 min and cooled to 80 °C in flowing He. At this temperature, sufficient CO_2 was injected until adsorption saturation, followed by purging with He (30 mL min^{-1}) for about 2 h. The temperature was then raised from 80 °C to 800 °C at a ramp rate of 5 °C min^{-1} to desorb CO_2. The desorbed CO_2 was detected by online gas chromatography with a TCD. Desorption amount of CO_2 was absorbed by NaOH solution followed by titration with hydrochloric acid standard solution with phenolphthalein and methyl orange as dual-indicator. The basicity of the catalyst is the amount of CO_2 absorbed by catalyst on unit weight (μmol g^{-1}). The acidity of catalyst was determined by NH_3-TPD experiment. The procedures were similar to CO_2-TPD experiment. Desorption amount of NH_3 was absorbed by HCl solution followed by titration with sodium hydroxide standard solution with phenolphthalein and methyl orange as dual-indicator. The acidity of the catalyst is the amount of NH_3 absorbed by catalyst on unit weight (μmol g^{-1}).

The DRIFT measurements of CO adsorption were carried out on a Bruker Vector 22 FTIR spectrometer equipped with a MCT detector and Harrick diffuse reflectance accessory. Spectra were obtained on a homemade apparatus loaded with 0.05 g of catalyst. Prior to the saturated adsorption of 0.5 vol% CO/He at room temperature, sample was subjected to the pretreatment with Helium flow at 200 °C for removing any other gases and moisture. Each spectrum was obtained after the 10 min evacuation treatment with Helium flow at 25 °C and by subtracting the background (base spectrum) of the unloaded sample.

In situ DRIFT measurements were performed in a Harrick diffuse reflectance infrared cell equipped with CaF_2 windows and adapted to the Nicolet FTIR/R760 spectrometer. Spectra were obtained on the apparatus loaded with 0.05 g of sample recording at 4 cm^{-1} resolution with 128 scans. Prior to the adsorption of HCOOD gas (bubbled with 20 mL min^{-1} of Helium at 10 °C, HCOOD content was ~2%), the sample was subjected to the pretreatment with Helium flow at 200 °C for removing moisture and any other gases. Each spectrum was obtained under the treatment with Helium flow at the indicated temperature and evacuated time, and by subtracting the background (base spectrum) of the unloaded sample.

2.3. Catalytic activity test

All catalytic experiments in open system were carried out under ambient atmosphere of air. Noted that the inert atmosphere of N_2 gave essentially the same rate of H_2 generation as air in this reaction. All reactions, unless otherwise stated, were conducted in a 10 mL double-walled thermostatically controlled reaction vessel under steady magnetic stirring (800 rpm) at the given temperature with a reflux condenser, which is connected to an automatic gas burette, where the gases are collected and temperature kept constant at 25 °C during measurements. The gas burette is equipped with a pressure sensor. Generating gas during the reaction causes a pressure increase in closed system, which is compensated by volume increase of the burette syringe by an automatic controlling unit. The gas generation curves are collected by a personal computer. There is a two piston burette for measurements above 100 mL. In addition, generated gas was qualitatively and quantitatively analyzed by GC (Agilent 6820 with a TDX-01 column connected to a TCD). Typically a ratio of H_2 and CO_2 of 1:1 (±5%) is detected. The reaction rates were calculated based on total gold atoms.

The catalytic experiment in closed system was carried out in a 50 mL Hastelloy-C high-pressure Parr autoclave. Typically, 5.0 mL scale of FA solution and calculated amount of Au catalyst were placed in the autoclave. Then it was sealed and the internal air was degassed completely using N_2 at room temperature. The stirrer was started with the rate of 800 rpm when the desired temperature of 80 °C was reached.

For the catalyst reuse experiment, the catalysts from parallel activity tests were collected, centrifuged and washed with deionized water, followed by drying at 100 °C in air for 1 h and reduction with a stream of 5 vol% H_2/Ar at 300 °C for 2 h. All catalytic activity tests were performed by following the same procedure as described above. To verify whether there is any leaching of zirconia or gold during the catalytic FA decomposition, the gold catalyst was removed from the reaction system by filtration after 3 h reaction. Analysis of the filtrate by ICP showed no detectable leaching of Zr or Au (<2.5 ppb) into the solution.

All kinetic isotope effect (KIE) experiments were carried out by using the same procedure as described above. The deuterium-labeled formic acid was purified by anhydrous $CuSO_4$ and/or D_2O were introduced into the reaction system. The isotope distribution for generated hydrogen gas was performed by dividing the effluent into two parallel streams: one was analyzed by a mass spectrometer (Balzers OmniStar) and the other by a GC (Agilent 6820 with a TDX-01 column connected to a TCD). Typically a ratio of hydrogen (H_2 or D_2 or HD) and carbon dioxide of 1:1 (±5%) is detected.

3. Results and discussion

3.1. Catalytic hydrogen generation from formic acid

In the course of our continuing efforts in developing green catalysis for clean hydrogen generation via aqueous formic acid decomposition, we have discovered an efficient approach achieving this particular goal under mild conditions and in the absence of volatile organic amines (VOCs). Based on our previous work [45], we used the biphasic zirconia (*b*-ZrO_2) supported gold catalyst (Au/*b*-ZrO_2, mean gold particle size ~ 1.8 nm) in 10.5 M additive-free aqueous FA at 40 °C, but no gas can be detected. Interestingly, appreciable catalytic activity with initial reaction rate of 50.6 L H_2 g_{Au}^{-1} h^{-1} was observed once the reaction temperature was elevated to 80 °C. In order to improve the performance of gold catalyst and investigate the amphoteric nature of ZrO_2 with different pure crystallite phases, we prepared and evaluated a series of zirconia polymorphs supported gold catalysts including Au/*m*-ZrO_2, Au/*t*-ZrO_2, and Au/*a*-ZrO_2. As shown in Fig. 1, a dramatic effect of the support polymorphs was found. Remarkably, Au supported on *m*-ZrO_2 was shown to be most active and selective for FA dehydrogenation in acidic medium, with an initial rate of up to 81.8 L H_2 g_{Au}^{-1} h^{-1} at 80 °C achievable for the exclusive formation of H_2 and CO_2 (Fig. 1a). The Au/*a*-ZrO_2 catalyst exhibited less activity with the rate of 47.8 L H_2 g_{Au}^{-1} h^{-1}, and Au/*t*-ZrO_2 showed the lowest performance of only 25.6 L H_2 g_{Au}^{-1} h^{-1}. There is also a significant difference from the long-term reaction profiles of FA dehydrogenation among the supported gold catalysts, that is, Au NPs on *m*-ZrO_2 are about 3.7 times more active than that of a similar size on *t*-

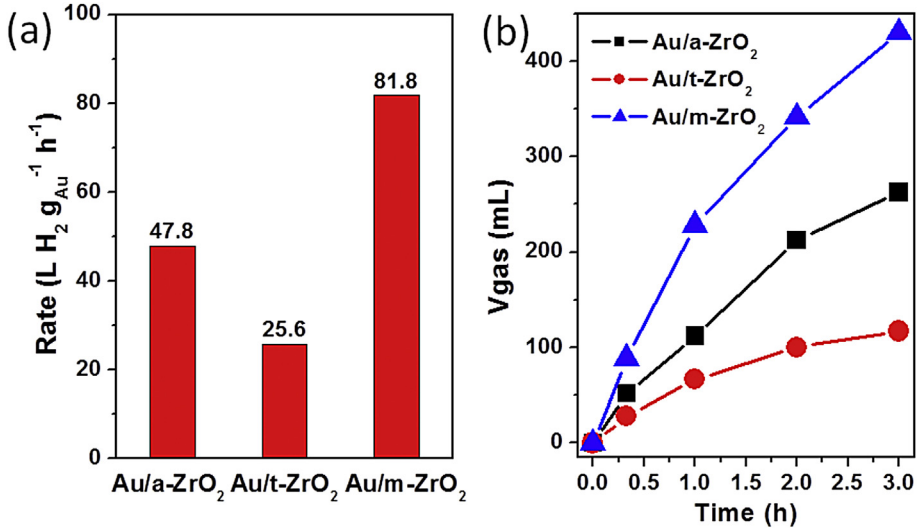

Fig. 1. Additive-free FA dehydrogenation over supported Au catalysts in open system. (a) Initial rate after 20 min, and (b) Profiles of evolved gas in 3 h. Reaction conditions: 5.0 mL scale of 10.5 M FA, n(FA)/n(Au) = 7000, 80 °C.

ZrO_2, as shown in Fig. 1b. The evolved gas in 3 h was 430.1, 262.3 and 117.1 mL for Au/m-ZrO_2, Au/a-ZrO_2 and Au/t-ZrO_2, respectively, on the indicated conditions. It should be emphasized that the performance of Au/m-ZrO_2 catalyst for additive-free aqueous FA dehydrogenation was comparable with the most active heterogeneous catalyst systems previously reported at temperatures of 20–92 °C [25,26,31–35]. In addition, the CO concentration was less than 9 ppm for these gold catalysts at 80 °C based on the gas stream after CO_2 removal using the GC-FID-Methanizer method.

The catalytic behaviors of ZrO_2 supported gold catalysts for FA decomposition in closed system was different from these in open one (Fig. 2). For these three gold catalysts, the initial rates in closed system were lower than the corresponding open system may due to the latter favoring the proceeding of FA dehydrogenation (Fig. 2a). The reaction rate of 68.6 L H_2 g_{Au}^{-1} h^{-1} at 80 °C for Au/m-ZrO_2 was much lower than that of 81.8 L H_2 g_{Au}^{-1} h^{-1} in open system. The Au/a-ZrO_2 and Au/t-ZrO_2 also showed lower catalytic activity of 45.3 and 24.7 L H_2 g_{Au}^{-1} h^{-1}, respectively. In longer reaction time, the pressure of evolved gas may exceed 5.9 MPa at 80 °C for Au/m-ZrO_2 sample, with the FA decomposition being allowed to go to completion (>95%) in an isolated process performed in the closed system, as shown in Fig. 2b. No significant inhibition of catalytic activity was observed up to the high pressure at near-ambient conditions. Au/a-ZrO_2 displayed robustly catalytic performance which was comparable with Au/m-ZrO_2 catalyst for FA dehydrogenation under the same reaction conditions.

To further investigate the different catalytic behaviors of zirconia polymorphs supported gold catalysts, the reusabilities of Au/m-ZrO_2 and Au/t-ZrO_2 in both open and closed systems were studied. Through chemical analysis by atomic absorption of the filtrates, the leaching of gold or ZrO_2 under such highly acidic environment and whether or in high-pressure was negligible, verifying the inherent stability of the ZrO_2 supported gold catalysts. For the Au/m-ZrO_2, the activity of the second reuse lowered by about 12.6% compared to the fresh one in open system, but the value was 24.9% in closed system (Fig. 3a and c). For the Au/t-ZrO_2 catalyst, the decreasing

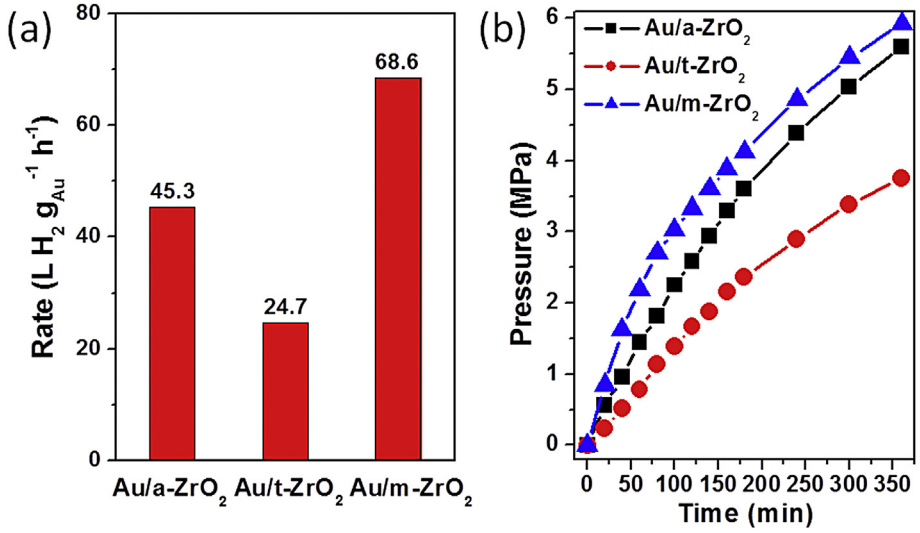

Fig. 2. Additive-free FA dehydrogenation over supported Au catalysts in closed system. (a) Initial rate after 1 h, and (b) Profiles of pressure variation in 6 h. Reaction conditions: 5.0 mL scale of 10.5 M FA, n(FA)/n(Au) = 1750, 80 °C.

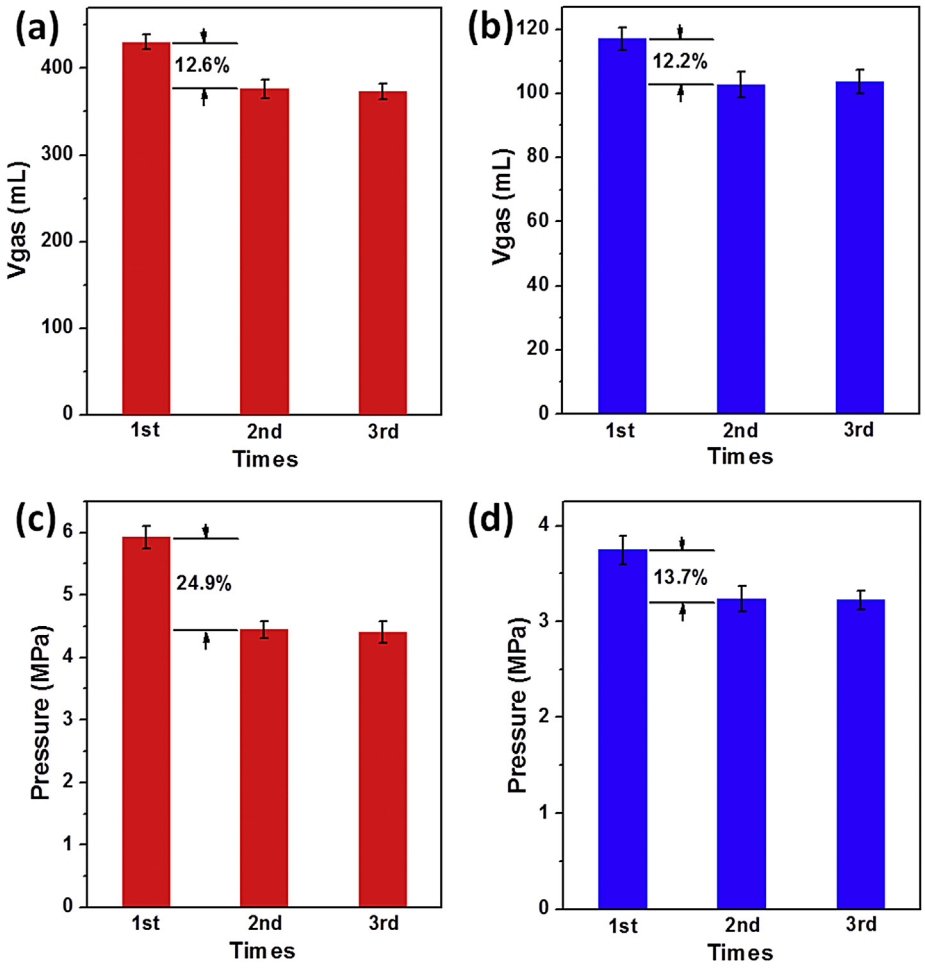

Fig. 3. Reuse of Au/*m*-ZrO_2 (left side, red column) and Au/*t*-ZrO_2 (right side, blue column) catalysts for hydrogen generation via decomposition of base-free aqueous FA. Reaction conditions: (a) and (b) in open reaction system, 5.0 mL scale of 10.5 M FA, *n*(FA)/*n*(Au) = 7000, 80 °C, 3 h in each run. (c) and (d) in closed reaction system, 5.0 mL scale of 10.5 M FA, *n*(FA)/*n*(Au) = 1750, 80 °C, 6 h in each run. Three separate experiments were performed for each plot; standard deviation error bars are shown. (For interpretation of the references to colour in this figure legend, the reader is referred to the web version of this article.)

amplitude was about 12.2% and only 13.7% in open and closed system, respectively (Fig. 3b and d). Interestingly, both catalysts showed good stability after the 2nd reuse either in open reaction system or in closed one. These results show that high-pressure in closed system exhibited more significant effect for Au/*m*-ZrO_2 catalyst on base-free aqueous FA decomposition. The remarkable loss of activity for Au/*m*-ZrO_2 catalyst in closed system excluded the influence of leaching of active metal or support and gold sintering (the mean size of Au NPs of used Au/*m*-ZrO_2 catalyst was ca. 2.1 nm) but probably due to the inevitable product of pressurized CO_2 which can be more easily adsorbed on the surface basic sites, and the formed carbonate species can cover the active sites of gold catalysts.

3.2. Structural characterization and surface acid-base property measurement

To ascertain the reason of the difference on catalytic activity of these zirconia polymorphs supported gold catalysts, the comprehensive investigation on microstructures and physiochemical properties were further carried out. The powder XRD patterns in Fig. 4 clearly show the well-defined crystal of monoclinic and tetragonal phase for pure *m*-ZrO_2 and *t*-ZrO_2, and the typical difference between these two ZrO_2 polymorphs. Intensive diffraction

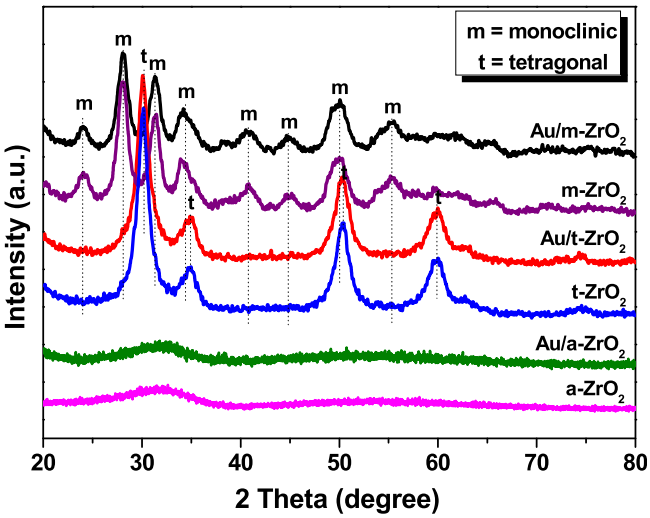

Fig. 4. XRD patterns of *a*-, *m*-, *t*-ZrO_2, and their supported Au catalysts.

patterns at 2θ of 24.1°, 28.1°, 31.3°, 34.4°, 40.8°, 44.8°, 50.0°, and 55.3° of *m*-ZrO_2 crystal phase (JCPDS 37-1484) are detected [46,47]. The peaks at 2θ of 30.2°, 34.9°, 50.4°, and 59.9° are diffraction

patterns of *t*-ZrO_2 crystal phase (JCPDS 50-1089) [46,47]. A broad X-ray diffraction line is observed for *a*-ZrO_2 sample, demonstrating an amorphous ZrO_2 with poor crystallinity. There are no structural changes after the loading of gold for the corresponding support, especially the phase transformation. The absence of any Au-containing crystal phases suggests the low gold loadings and high dispersion of the gold species. The crystallite size of *m*-ZrO_2 and *t*-ZrO_2 were calculated using Scherrer formula to be 9.2 and 10.3 nm from the major diffraction peaks at 28 and 30°, respectively. Nitrogen adsorption isotherms at −196 °C gave BET surface area values ranging from 109 $m^2\ g^{-1}$ for the sample of *t*-ZrO_2 to 186 $m^2\ g^{-1}$ for *a*-ZrO_2 (Table 1), which are in good agreement with the previously reported results [46–48]. Meanwhile, gold deposition can lead to the slight decrease of specific surface area for the underlying ZrO_2 support. The data of pore volume and pore diameter show a typical mesoporous feature of these supports and gold catalysts.

The gold loading on Au/*a*-ZrO_2, Au/*m*-ZrO_2 and Au/*t*-ZrO_2 was respective 0.75, 0.80 and 0.68 wt% according to the ICP-AES technique (Table 1). TEM and HAADF-STEM images and STEM-EDX mappings in Fig. 5 and Fig. S1-3 show that the gold NPs uniformly and highly dispersed on the corresponding supports with comparable particle size of 2.3, 2.0, and 2.2 nm for Au/*a*-ZrO_2, Au/*m*-ZrO_2, and Au/*t*-ZrO_2 catalyst, respectively. Meanwhile, the binding energy of 87.4 eV for $4f_{5/2}$ and 83.7 eV for $4f_{2/7}$ clearly demonstrate that there is only metallic gold on the surface of these Au-supported samples (Fig. 6a) [45]. The fact that no bands for Au^+ or $Au^{\delta+}$ can be seen from the DRIFT spectra of CO adsorption, as presented in Fig. 6b, further confirms the exclusive presence of metallic Au species in these materials [45].

Based on the above textural characterization results, the difference of activity for these ZrO_2 polymorphs supported gold catalysts would exclude the effect of surface area, Au particle size, oxidation state of surface active sites, probably because the surface acid-base property of samples [49,50]. The acidity measurements of ZrO_2 supports and supported Au catalysts were carried out by NH_3-TPD. There is no significant difference on the nature of acidic sites for the ZrO_2 with different polymorphs as well as the corresponding supported gold catalysts, as shown in Fig. 7a. For supports, there are two desorption peaks at 150 °C and a broad one at 445 °C ascribed respectively to weak and strong surface acidic sites [49], and *a*-ZrO_2 shows the largest amount of surface acidic sites while *t*-ZrO_2 exhibits the least one. But for the gold catalysts, there are three desorption peaks at 150, 400 and 554 °C, indicative of more strong acidic sites compared to the corresponding supports. The amount of total surface acidic sites for Au/*a*-ZrO_2, Au/*m*-ZrO_2 and Au/*t*-ZrO_2 samples determined with the titration method are 161.8, 129.4 and 92.5 μmol g^{-1}, respectively. On the other hand, the basicity measurements of ZrO_2 supports and supported Au catalysts were carried out by CO_2-TPD. There are two desorption peaks at around 130 and 450 °C ascribed respectively to the weak and strong surface basic sites for the ZrO_2 supports [49], as shown in Fig. 7b. The Au deposition displays no change on the nature of weak surface basic sites, but can induce the position of strong surface basic sites slight shifting to the higher value of 490 °C, indicative of the appearance of stronger surface basic sites. The amount of surface basic sites for gold supported on *m*-ZrO_2, *a*-ZrO_2 and *t*-ZrO_2 catalysts can also be quantitatively determined with the titration method are 78.7, 22.3 and 9.6 μmol g^{-1}, respectively, which are in good agreement with the previous report [51]. The above-mentioned surface acidity-basicity results suggest that ZrO_2 polymorphs supported gold catalysts can be considered as amphoteric matrixes, but Au/*m*-ZrO_2 presents much more base than other counterparts.

3.3. Active sites and structure-activity relationships

Many workers reported that *m*-ZrO_2 and *t*-ZrO_2 possess different amount of acidity and basicity due to the distinction of surface hydroxyl, which can strongly influence the catalytic activities and selectivities for many reactions [49–54]. He et al. [52] elucidated that there was strong Lewis acidity of Zr^{4+} cations and the strong Lewis basicity of O^{2-} anions of coordinative unsaturated Zr^{4+}–O^{2-} pairs on the surface of *m*-ZrO_2. And the CO_2 adsorption capacity of *m*-ZrO_2 is more than an order of magnitude higher than that of *t*-ZrO_2. The *a*-ZrO_2 support was calcined at lower temperature of 300 °C possessed more OH groups thus showed large amount of surface acidic sites [52]. Generally, surface basicity could be crucial for the chemical reaction proceeding in acidic medium, e.g., FA dehydrogenation [45].

To further explore the intrinsically catalytic nature of different ZrO_2 polymorphs supported gold catalysts, the *in situ* DRIFTS technique for labeled FA was employed. The distinct IR results of various supported gold catalysts are shown in Fig. 8. The peaks at 2736, 2858 and 3686 cm^{-1} are ascribed to the IR vibration of OD, CH and OH groups on the surface of supported gold catalysts, respectively [45]. The OD groups derived from the exchange of OH of supports and D-labeled FA of HCOOD. And the intensity of OH bond for Au/*m*-ZrO_2 was stronger than those of Au/*a*-ZrO_2 and Au/*t*-ZrO_2 catalysts, indicative of the more basic sites in former than in latter, which are consistent with the CO_2-TPD results above. Meanwhile, the OD bond intensity shows the similar trend of OH bond for these gold catalysts. These results indicate that the H/D exchange reaction over Au/*m*-ZrO_2 occurred with the highest rates than those over Au/*a*-ZrO_2 and Au/*t*-ZrO_2 catalysts. For the dehydrogenation of FA over the gold catalysts, it is widely accepted that the reaction initiates with the cleavage of O–H bond from HCOOH to yield formate and proton on the interface of metal and support [12–16,25,26,45]. And the H/D exchange between proton of FA and H atom from ZrO_2 surface can occur if HCOOD was used. Based on the findings of above CO_2-TPD, NH_3-TPD and HCOOD-IR, it can be concluded that basic sites exhibited significant effect on the catalytic performance of aqueous FA decomposition reaction, that is, the higher population of basic sites for Au/*m*-ZrO_2 sample, the faster reaction rate for FA dehydrogenation.

To gain a further mechanistic understanding of this key aspect, the experiments in which one hydrogen atom in FA being labeled with deuterium and the effect of solvents were carried out. The rate

Table 1
Characteristics of the ZrO_2 supports and gold catalysts.

Sample	Surface area ($m^2\ g^{-1}$)	Pore volume ($cm^3\ g^{-1}$)	Pore diameter (nm)	Au loading (wt%)	Au particle size (nm)
a-ZrO_2	186	0.3538	8.3	–	–
m-ZrO_2	137	0.3075	8.9	–	–
t-ZrO_2	109	0.2756	10.1	–	–
Au/*a*-ZrO_2	172	0.2339	7.6	0.75	2.3
Au/*m*-ZrO_2	118	0.1825	8.2	0.80	2.0
Au/*t*-ZrO_2	106	0.2033	9.4	0.68	2.2

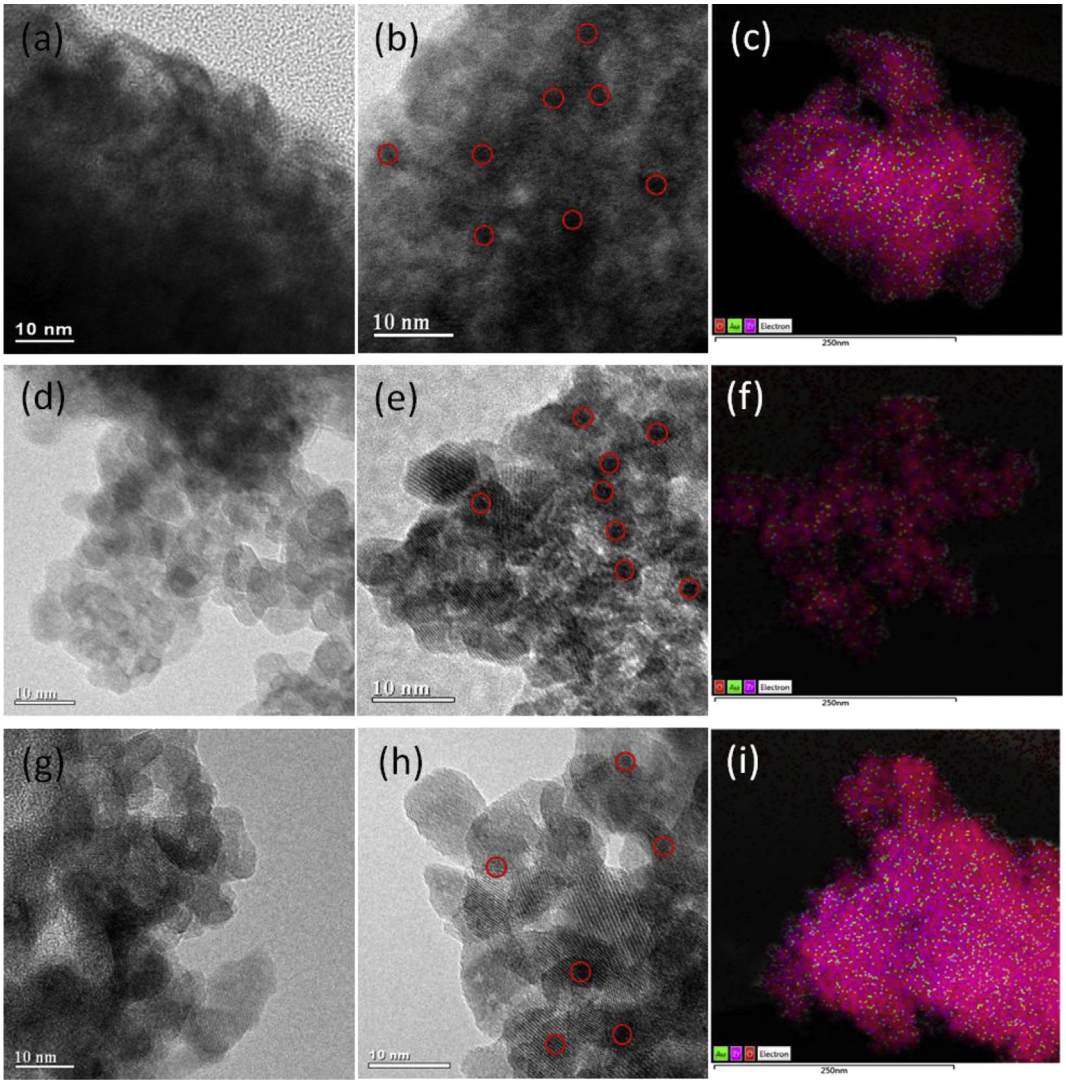

Fig. 5. TEM images of (a) *a*-ZrO_2, (b) Au/*a*-ZrO_2, (d) *m*-ZrO_2, (e) Au/*m*-ZrO_2, (g) *t*-ZrO_2, and (h) Au/t-ZrO_2, and STEM-EDX mappings of (c) Au/*a*-ZrO_2, (f) Au/*m*-ZrO_2, and (i) Au/*t*-ZrO_2.

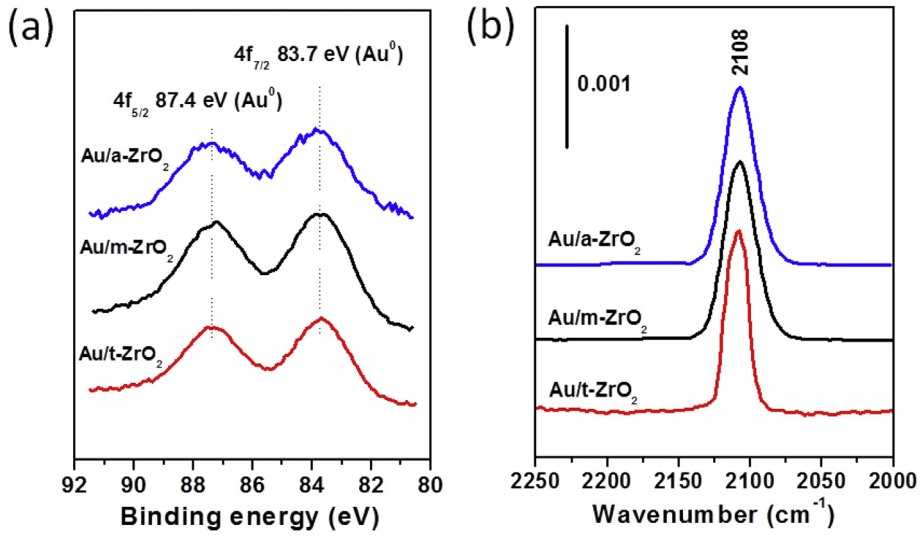

Fig. 6. (a) Binding energies and (b) CO-DRIFT spectra of Au° for gold catalysts.

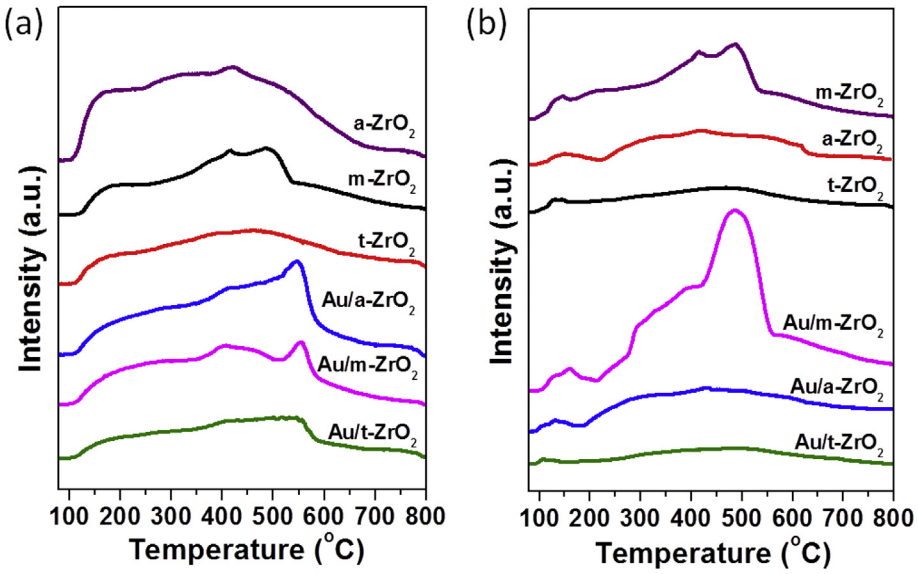

Fig. 7. (a) NH_3-TPD and (b) CO_2-TPD profiles of ZrO_2 supports and supported Au catalysts.

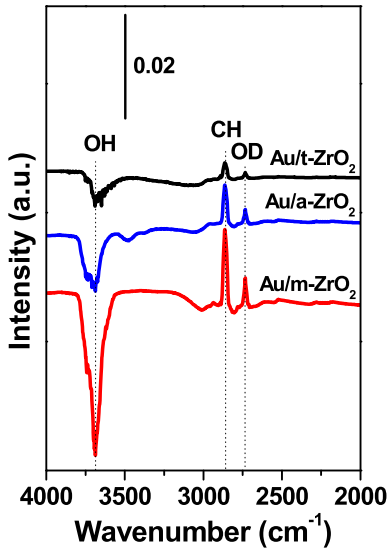

Fig. 8. DRIFT spectra of H/D exchange of HCOOD with surface OH groups of the catalysts at 80 °C (recorded after a 15-min exposure to 2% HCOOD in Helium gas).

of H_2 evolution, kinetic isotope effects (KIEs), and isotope distributions for evolved hydrogen gas in decomposition of FA by supported gold catalysts are listed in Table 2. Although D-labeled formic acid showed significant KIEs in the process of chemical reaction over both catalysts, HCOOD and DCOOH exhibited slight KIEs each other, indicative of the cleavage of O–H and H–C bonds is kinetically-relevant step in aqueous FA solution [45]. The reaction rate of Au/*m*-ZrO_2 was much higher than that of Au/*t*-ZrO_2 under identical reaction conditions, which also attributed to a higher population of surface basic sites of the former than latter and are in agreement with the CO_2-TPD results. It is interesting to find that there are some differences for the fraction of H_2, D_2, and HD in the evolved hydrogen gas, inferring that H_2O may participate in the FA dehydrogenation process (hydrogen atoms originate from both the acid and water molecules). To explore the possibility, the reaction solvent was changed to be D_2O instead of H_2O (Table 2). There are some D_2 and HD components in spite of D-labeled formic acid free

Table 2
Rate of H_2 evolution, KIEs, and isotope distributions for evolved hydrogen gas in decomposition of FA catalyzed by supported gold catalysts.[a]

Entry	Catalyst	Formic acid	Rate ($L\ H_2\ g_{Au}^{-1}\ h^{-1}$)	KIE	Fraction (mol%)		
					H_2	D_2	HD
1	Au/*m*-ZrO_2	HCOOH	76.8	–	100	0	0
2	Au/*m*-ZrO_2	HCOOD	30.6	2.5	18	0	82
3	Au/*m*-ZrO_2	DCOOH	26.3	2.9	8	0	92
4	Au/*t*-ZrO_2	HCOOH	21.3	–	100	0	0
5	Au/*t*-ZrO_2	HCOOD	7.9	2.7	10	0	90
6	Au/*t*-ZrO_2	DCOOH	7.3	2.9	8	0	92
7[b]	Au/*m*-ZrO_2	HCOOH	71.2	–	79	5	16
8[b]	Au/*m*-ZrO_2	DCOOH	12.7	–	0	15	85

[a] Reaction conditions: 5.0 mL scale of 10.5 M FA, n(FA)/n(Au) = 7000, 80 °C, 1 h.
[b] D_2O as the solvent instead of H_2O.

in the reactant, indicative of the existence of H/D exchange between FA and solvent such as H_2O or D_2O [55,56], following the reaction pathways as shown below [45].

$$HCOOH + 2Au \leftrightarrow (HCOO{-}Au)^- + (Au{-}H)^+ \quad (1)$$

$$(HCOO{-}Au)^- \rightarrow (Au{-}H)^- + CO_2 \quad (2)$$

$$(Au{-}H)^+ + (Au{-}H)^- \rightarrow H_2 + 2Au \quad (3)$$

$$D_2O \leftrightarrow D^+ + OD^- \quad (4)$$

$$(Au{-}H)^- + D^+ \rightarrow HD + Au \quad (5)$$

$$(Au{-}H)^+ + OD^- \rightarrow HDO + Au \quad (6)$$

The dehydrogenation rate of HCOOH in D_2O was slightly lower than that of HCOOH in H_2O, but significantly higher than other reaction systems which containing D-labeled substrates. The reaction rate of DCOOH dehydrogenation in both D_2O and Au/*m*-ZrO_2 system was very low due to the double D-labeled effect [55]. Overall, the reaction rate decreases in the following order: [HCOOH + H_2O] > [HCOOH + D_2O] > [DCOOH + H_2O] > [DCOOH + D_2O], which can be reasonably explained with an H/D exchange between FA and water and the double D-labeled effect.

4. Conclusions

Gold nanoparticles supported on ZrO_2 polymorphs are found to be active and selective catalysts for base-free aqueous FA decomposition for ultrahigh clean H_2 gas under mild conditions. With comparable gold particle size, Au/*m*-ZrO_2 can much more favorably facilitate FA deprotonation which appears to be a key factor for achieving high activity in the desired reaction. The promotion effect was mainly ascribed to the much more density of surface basic sites on Au/*m*-ZrO_2 compared with Au/*a*-ZrO_2 and Au/*t*-ZrO_2. On the other hand, more significant loss of activity in the second run in closed and pressurized system can be observed over Au/*m*-ZrO_2 sample due to the inevitable product of CO_2 could be more easily adsorbed on the surface basic sites. During the process of base-free aqueous FA dehydrogenation, there was an existence of H/D exchange reaction between solvent of H_2O and substrate of HCOOH. These results may contribute to the design of more efficient metal-based catalytic systems, especially on heterogeneous gold catalysis, for clean energy storage/distribution and extended applications of FA in renewable chemical processes.

Acknowledgements

This work was financially supported by the National Natural Science Foundation of China (Grants 21273044, 21473035, 91545108, and 51502331), and the Science and Technology Commission of Shanghai (Grant 16ZR1440400). The authors declare no competing financial interests.

Appendix A. Supplementary data

Supplementary data related to this article can be found at http://dx.doi.org/10.1016/j.jpowsour.2016.08.056.

References

[1] S. Enthaler, ChemSusChem 1 (2008) 801–804.
[2] F. Joó, ChemSusChem 1 (2008) 805–808.
[3] K.M.K. Yu, I. Curcic, J. Gabriel, S.C.E. Tsang, ChemSusChem 1 (2008) 893–899.
[4] H.L. Jiang, S.K. Singh, J.M. Yan, X.B. Zhang, Q. Xu, ChemSusChem 3 (2010) 541–549.
[5] L. Schlapbach, A. Züttel, Nature 414 (2001) 353–358.
[6] M. Aresta, A. Dibenedetto, A. Angelini, Chem. Rev. 114 (2014) 1709–1742.
[7] H. Tian, Q. Guo, D. Xu, J. Power Sour. 195 (2010) 2136–2142.
[8] K. Fujita, Y. Tanaka, M. Kobayashi, R. Yamaguchi, J. Am. Chem. Soc. 136 (2014) 4829–4832.
[9] P.Z. Li, A. Aijaz, Q. Xu, Angew. Chem. Int. Ed. 51 (2012) 6753–6756.
[10] M. Nielsen, E. Alberico, W. Baumann, H.J. Drexler, H. Junge, S. Gladiali, M. Beller, Nature 495 (2013) 85–89.
[11] L. He, Y. Huang, A. Wang, X. Wang, X. Chen, J.J. Delgado, T. Zhang, Angew. Chem. Int. Ed. 51 (2012) 6191–6194.
[12] F. Solymosi, Á. Koós, N. Liliom, I. Ugrai, J. Catal. 279 (2011) 213–219.
[13] K. Tedsree, A.T.S. Kong, S.C. Tsang, Angew. Chem. Int. Ed. 48 (2009) 1443–1446.
[14] M. Ojeda, E. Iglesia, Angew. Chem. Int. Ed. 48 (2009) 4800–4803.
[15] K. Tedsree, C.W.A. Chan, S. Jones, Q. Cuan, W.K. Li, X.Q. Gong, S.C.E. Tsang, Science 332 (2011) 224–228.
[16] Y. Karatas, A. Bulut, M. Yurderi, I.E. Ertas, O. Alal, M. Gulcan, M. Celebi, H. Kivrak, M. Kaya, M. Zahmakiran, Appl. Catal. B 180 (2016) 586–595.
[17] A. Boddien, C. Federsel, P. Sponholz, D. Mellmann, R. Jackstell, H. Junge, G. Laurenczy, M. Beller, Energy Environ. Sci. 5 (2012) 8907–8911.
[18] B. Loges, A. Boddien, H. Junge, M. Beller, Angew. Chem. Int. Ed. 47 (2008) 3962–3965.
[19] C. Fellay, P.J. Dyson, G. Laurenczy, Angew. Chem. Int. Ed. 47 (2008) 3966–3968.
[20] Y. Maenaka, T. Suenobu, S. Fukuzumi, Energy Environ. Sci. 5 (2012) 7360–7367.
[21] J.F. Hull, Y. Himeda, W.H. Wang, B. Hashiguchi, R. Periana, D.J. Szalda, J.T. Muckerman, E. Fujita, Nat. Chem. 4 (2012) 383–388.
[22] M. Grasemann, G. Laurenczy, Energy Environ. Sci. 5 (2012) 8171–8181.
[23] A. Boddien, D. Mellmann, F. Gärtner, R. Jackstell, H. Junge, P.J. Dyson, G. Laurenczy, R. Ludwig, M. Beller, Science 333 (2011) 1733–1736.
[24] E.A. Bielinski, P.O. Lagaditis, Y. Zhang, B.Q. Mercado, C. Würtele, W.H. Bernskoetter, N. Hazari, S. Schneider, J. Am. Chem. Soc. 136 (2014) 10234–10237.
[25] S. Jones, J. Qu, K. Tedsree, X.Q. Gong, S.C.E. Tsang, Angew. Chem. Int. Ed. 51 (2012) 11275–11278.
[26] K. Tedsree, T. Li, S. Jones, C.W.A. Chan, K.M.K. Yu, P.A.J. Bagot, E.A. Marquis, G.D.W. Smith, S.C.E. Tsang, Nat. Nanotech. 6 (2011) 302–307.
[27] X.J. Gu, Z.H. Lu, H.L. Jiang, T. Akita, Q. Xu, J. Am. Chem. Soc. 133 (2011) 11822–11825.
[28] Y. Chen, Q.L. Zhu, N. Tsumori, Q. Xu, J. Am. Chem. Soc. 137 (2015) 106–109.
[29] Q.L. Zhu, N. Tsumori, Q. Xu, J. Am. Chem. Soc. 137 (2015) 11743–11748.
[30] K. Jiang, K. Xu, S. Zou, W.B. Cai, J. Am. Chem. Soc. 136 (2014) 4861–4864.
[31] Y.Y. Cai, X.H. Li, Y.N. Zhang, X. Wei, K.X. Wang, J.S. Chen, Angew. Chem. Int. Ed. 52 (2013) 11822–11825.
[32] S. Zhang, Ö. Metin, D. Su, S. Sun, Angew. Chem. Int. Ed. 52 (2013) 3681–3684.
[33] Z.L. Wang, J.M. Yan, Y. Ping, H.L. Wang, W.T. Zheng, Q. Jiang, Angew. Chem. Int. Ed. 52 (2013) 4406–4409.
[34] J.M. Yan, Z.L. Wang, L. Gu, S.J. Li, H.L. Wang, W.T. Zheng, Q. Jiang, Adv. Energy Mater. (2015) 1500107.
[35] Q. Liu, X. Yang, Y. Huang, S. Xu, X. Su, X. Pan, J. Xu, A. Wang, C. Liang, X. Wang, T. Zhang, Energy Environ. Sci. 8 (2015) 3204–3207.
[36] X. Zhou, Y. Huang, W. Xing, C. Liu, J. Liao, T. Lu, Chem. Commun. 30 (2008) 3540–3542.
[37] X. Wang, G.W. Qi, C.H. Tan, Y.P. Li, J. Guo, X.J. Pang, S.Y. Zhang, Int. J. Hydrogen Energy 39 (2014) 837–843.
[38] H. Dai, B. Xia, L. Wen, C. Du, J. Su, W. Luo, G. Cheng, Appl. Catal. B 165 (2015) 57–62.
[39] J. Liu, L. Lan, R. Li, X. Liu, C. Wu, Int. J. Hydrogen Energy 41 (2016) 951–958.
[40] Q.Y. Bi, J.D. Lin, Y.M. Liu, X.L. Du, J.Q. Wang, H.Y. He, Y. Cao, Angew. Chem. Int. Ed. 53 (2014) 13583–13587.
[41] M. Haruta, T. Kobayashi, H. Sano, N. Yamada, Chem. Lett. 16 (1987) 405–408.
[42] M. Yang, L.F. Allard, M. Flytzani-Stephanopoulos, J. Am. Chem. Soc. 135 (2013) 3768–3771.
[43] A. Wittstock, V. Zielasek, J. Biener, C.M. Friend, M. Bäumer, Science 327 (2010) 319–322.
[44] X. Liu, L. He, Y.M. Liu, Y. Cao, Acc. Chem. Res. 47 (2014) 793–804.
[45] Q.Y. Bi, X.L. Du, Y.M. Liu, Y. Cao, H.Y. He, K.N. Fan, J. Am. Chem. Soc. 134 (2012) 8926–8933.
[46] W. Li, H. Huang, H. Li, W. Zhang, H. Liu, Langmuir 24 (2008) 8358–8366.
[47] P.M. de Souza, R.C. Rabelo-Neto, L.E.P. Borges, G. Jacobs, B.H. Davis, U.M. Graham, D.E. Resasco, F.B. Noronha, ACS Catal. 5 (2015) 7385–7398.
[48] A.G. Sato, D.P. Volanti, D.M. Meira, S. Damyanova, E. Longo, J.M.C. Bueno, J. Catal. 307 (2013) 1–17.
[49] Y. Li, D. He, Q. Zhu, X. Zhang, B. Xu, J. Catal. 221 (2004) 584–593.
[50] P.O. Graf, D.J.M. de Vlieger, B.L. Mojet, L. Lefferts, J. Catal. 262 (2009) 181–187.
[51] N.F.P. Ribeiro, F.M.T. Mendes, C.A.C. Perez, M.M.V.M. Souza, M. Schmal, Appl. Catal. A 347 (2008) 62–71.
[52] D. He, Y. Ding, H. Luo, C. Li, J. Mol. Catal. A 208 (2004) 267–271.
[53] M.D. Rhodes, A.T. Bell, J. Catal. 233 (2005) 198–209.
[54] X. Zhang, H. Shi, B.Q. Xu, J. Catal. 279 (2011) 75–87.
[55] H. Wiener, Y. Sasson, J. Mol. Catal. 35 (1986) 277–284.
[56] B. Zaidman, H. Wiener, Y. Sasson, Int. J. Hydrogen Energy 11 (1986) 341–347.